

WAVE ATOM BASED COMPRESSIVE SENSING AND ADAPTIVE BEAMFORMING IN ULTRASOUND IMAGING

Foroohar Foroozan* and Parastoo Sadeghi**

*InnoMind Technology, Toronto, Canada, **Research School of Engineering, Australian National University, Canberra, Australia

ABSTRACT

The paper investigates combining Compressive Sensing (CS) with the robust Capon beamformer (RCB) for the purpose of medical ultrasound image formation with a much reduced number of samples compared to those used in current state-of-art ultrasound. The proposed CS algorithm uses wave atom dictionary as a low dimension projection, a Bernouli random matrix as a sensing matrix and a regularized- l_1 optimization technique for recovery. The reconstructed signals are then pre-processed before using the RCB technique augmented with spatial smoothing and diagonal loading. This approach is demonstrated through simulations, wire phantom and *in vivo* cardiac data with a reduction of up to 1/8 in the processed data rate and ultrasound images of similar perceived quality.

Index Terms— Compressive Sensing, Robust Capon Beamforming, Wave Atom, Delay-and-Sum.

1. INTRODUCTION

Diagnostic ultrasound acquires images from the body tissues by sending acoustic beams and collecting the scattered waves by an array of transducers, which are then processed by a beamforming technique to increase the signal-to-noise ratio (SNR). Being portable, real-time, risk free and relatively cheap, ultrasound imaging is modality of common choice for physicians. However, in ultrasound, sometimes there is the need for a large number of transducers (sometimes as high as a couple of thousands) producing several hundreds of frame rate per second, each consisting of several of hundreds of image lines [1]. Therefore, they have to process a large amount of data with high quality. Delay-and-Sum (DAS) [2] is a preferred beamforming method in current ultrasound machines. In the DAS approach, relevant time-of-flights from each transducer element to each point in the region of interest (ROI) are compensated and then a summation is performed on all the aligned observations to form the image. The DAS beamformer is independent of data with fixed weights, therefore, it provides lower resolution and worse interference suppression capability as compared to the data-dependent techniques like the Capon beamformer [3]. A typical reason for not using adaptive beamformers in ultrasound is the mismatch between the presumed and the actual array responses due to imprecise knowledge of the transducer positions resulting in signal cancellation in situations where this mismatch is not addressed properly [4]. So, applying Capon to the ultrasound needs considerable changes in order to adapt it to this complex environment.

Compressive sensing (CS) approaches provide an alternative to the classical Nyquist sampling framework and enable signal reconstruction at lower sampling rates [5]. The idea of CS as proposed by Donoho is to merge the compression and sampling steps, i.e., “why to go through so much effort to acquire all the data when most of what we acquire will eventually be thrown away” [6]. In recent years, the area of CS has branched out to a number of new

fronts and has worked its way into several application areas, such as radar, communications, and ultrasound imaging. Eldar and her colleagues published extensively and profoundly in applying the CS theory to ultrasound imaging [7–9]. In all of these works, the DAS is considered as the basis for image reconstruction and the Fourier domain is selected as the sparse domain. When it comes to oscillatory signals like ultrasound waves, wave atom decompositions have been shown to have significantly sparser solution than other existing methods [10]. Wave atom for ultrasound has been recently studied in [11] but the method was tested using simulations and not real data. Further, the DAS is applied for image reconstruction and a basis pursuit (BP) problem [12] is used for recovery.

The prime focus of this paper is to apply the wave atom based CS to real diagnostic ultrasound data (to reduce the sampling rate) in conjunction with the RCB (to enhance the beamforming quality). As it is shown in Fig. 1, for low dimension signal acquisition, a Bernouli random sensing matrix is used which reduces the sampling rate of up to 1/8th of the original rate used by the Analog-to-Digital Converters (ADCs). For sparse representation, a wave atom basis is used. Generally speaking, wave atoms interpolates between directional wavelets [13] and Gabor [14] transforms. An optimization problem based on regularized- l_1 -norm is solved using the NESTA algorithm [15] to reconstruct the signals. Then, the reconstructed signals are beamformed using the RCB technique augmented with spatial smoothing and diagonal loading. Our simulated and experimental results are presented in order to accelerate the acquisition rate without dropping the quality in terms of image resolution.

The paper is organized as follows. Section 2 defines the notation and derives the mathematical formulation for ultrasound received signals in a multiple reflector environment followed by the formulation of the DAS and the RCB technique in the frequency domain. Section 3 provides the details of our applied CS technique based on the wave atom dictionary. In Section 4, we compare the results of applying the CS technique and adaptive beamforming to both the simulated signals as well as data obtained from an ultrasound machine using a wire phantom and *in vivo* cardiac data. Finally, section 5 concludes the paper.

2. SYSTEM MODEL AND IMAGE RECONSTRUCTION

In this model, the scatterers are assumed to be point reflectors producing the field $f(\mathbf{r}_s, t) = q(t)\delta(\mathbf{r}_s)$ due to an excitation probe sent by the transducers. The notation $\delta(\mathbf{r}_s)$ is the multidimensional Dirac delta function at point \mathbf{r}_s with a strength of $q(t)$ that depends on the probing signal and the forward path attenuation. The emissions from these reflectors are convolved with the Green’s function of the tissue recorded by the transducers at \mathbf{r}_m , for $(1 \leq m \leq M)$ and produces the following pressure field at the receiving elements.

$$p(\mathbf{r}_m, t') = g(\mathbf{r}, t|\mathbf{r}_m, t') \otimes f(\mathbf{r}_s, t), \quad (1)$$

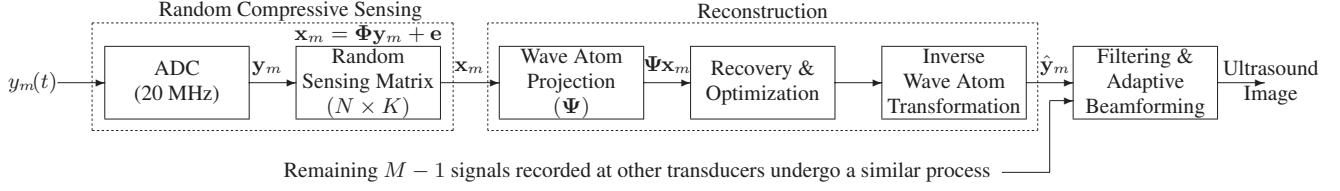


Fig. 1. Block diagram of the proposed overall system, including the random sensing matrix, signal reconstruction, and image formation through the RCB method. In practice, Analog-to-Digital Converter (ADC) and the sensing block becomes one entity, sampling with much lower rates than it is imposed by the Nyquist rate.

where the notation \otimes stands for convolution. With c denoting the propagation speed, the Green's function at time t' is [16]

$$g(\mathbf{r}, t | \mathbf{r}_m, t') = \frac{1}{4\pi|\mathbf{r} - \mathbf{r}_m|} \delta(|\mathbf{r} - \mathbf{r}_m|/c - (t - t')). \quad (2)$$

In the frequency domain, the recordings at transducers are denoted by $Y_m(\omega_q)$, ($1 \leq m \leq M$), for M transducers and Q frequency bins ($1 \leq q \leq Q$) which can be presented as

$$Y_m(\omega_q) = H_m(\omega_q)P(\mathbf{r}_m, \omega_q) + N_m(\omega_q), \quad (3)$$

where $H_m(\omega_q)$ is the frequency response of transducer m , $P(\mathbf{r}_m, \omega_q)$ is the pressure field at the receiver m in response to the transmitting wave, and $N_m(\omega_q)$ is the observation noise. In this model, the receivers are assumed to be point transducers. In practice, however, due to the limited size of the transducer, $H_m(\omega_q)$ is also space dependent. The pressure $P_m(\mathbf{r}_m, \omega_q)$ is the multiplication of frequency domain Green's function of the medium as defined in (2) and the source field generated from the scatterers at location \mathbf{r}_s denoted by $F(\mathbf{r}_s, \omega_q)$. Defining the *frequency dependent near field array steering vector* $\mathbf{a}(\mathbf{r}_s, \omega_q)$ as a collection of Green's functions (2) for the receive array as

$$\mathbf{a}(\mathbf{r}_s, \omega_q) \triangleq \left[\frac{e^{-j(\omega_q/c)|\mathbf{r}_s - \mathbf{r}_1|}}{4\pi|\mathbf{r}_s - \mathbf{r}_1|}, \dots, \frac{e^{-j(\omega_q/c)|\mathbf{r}_s - \mathbf{r}_M|}}{4\pi|\mathbf{r}_s - \mathbf{r}_M|} \right]^T, \quad (4)$$

the $(M \times 1)$ vector of received signals can be represented as

$$\mathbf{y}(\omega_q) = (\mathbf{h}(\omega_q) \odot \mathbf{a}(\mathbf{r}_s, \omega_q))F(\mathbf{r}_s, \omega_q) + \mathbf{n}(\omega_q), \quad (5)$$

with $\mathbf{y}(\omega_q) = [Y_1(\omega_q), \dots, Y_M(\omega_q)]^T$. Similarly, the vector $\mathbf{n}(\omega_q)$ is the stack vector of all the M observation noise $N_m(\omega_q)$, and the notation \odot is the Hadamard product of the two vectors. The $(M \times 1)$ vector $\mathbf{h}(\omega_q) = [\alpha(\mathbf{r}_1, \omega_q)H_1(\omega_q), \dots, \alpha(\mathbf{r}_M, \omega_q)H_M(\omega_q)]^T$ takes care of both the frequency dependent attenuation factors $\alpha(\mathbf{r}_m, \omega_q)$ of the environment as well as the frequency response of the transducers. For any observation point \mathbf{x} inside the ROI, the search steering vector is denoted by $\mathbf{a}(\mathbf{x}, \omega_q)$. With $\tilde{\mathbf{y}}(\omega_q)$ being the filtered vector of $\mathbf{y}(\omega_q)$, the non-coherent DAS beamforming results in the following image reconstructed from the recorded signals

$$I(\mathbf{x}) = (1/Q) \sum_{\omega_q} \mathbf{a}^H(\mathbf{x}, \omega_q) \tilde{\mathbf{y}}(\omega_q). \quad (6)$$

As previously discussed, the DAS beamforming suffers from high side lobe levels since its weights are fixed and are independent of the data. On the other hand, standard Capon beamforming suppresses the interfering signals by adaptively choosing a weight function based on the received signals to reconstruct the image using the following quadratic problem [17]

$$\min_{\mathbf{w}} \mathbf{w}^H \mathbf{R}(\omega_q) \mathbf{w} \quad \text{subject to} \quad \mathbf{w}^H \mathbf{a}(\mathbf{r}_s, \omega_q) = 1, \quad (7)$$

where the $M \times 1$ vector \mathbf{w} is the beamformer weight vector and the spatial covariance matrix is denoted by $\mathbf{R}(\omega_q)$. The solution to this problem is given as [18, 19]

$$\mathbf{w}(\mathbf{x}, \omega_q) = \frac{\mathbf{R}(\omega_q)^{-1} \mathbf{a}(\mathbf{x}, \omega_q)}{\mathbf{a}^H(\mathbf{x}, \omega_q) \mathbf{R}(\omega_q)^{-1} \mathbf{a}(\mathbf{x}, \omega_q)}. \quad (8)$$

Applying the weights \mathbf{w} , the coherent beamformed signal is

$$\mathbf{z} = (1/Q) \sum_{\omega_q} \mathbf{w}^H(\mathbf{x}, \omega_q) \tilde{\mathbf{y}}(\omega_q). \quad (9)$$

Due to the complex nature of the ultrasound, the Capon beamforming is applied with the following modifications to the real ultrasound data [1].

- **Robust adaptive beamforming:** The RCB proposed in [3, 17] overcomes the sensitivity of the standard capon to mismatch between the real and the presumed steering vectors. Assuming that the presumed steering vector is denoted by \mathbf{a} and the real one by $\bar{\mathbf{a}}$, a positive definite matrix by $\mathbf{B} = \epsilon \mathbf{I}$ (with ϵ defined in (10)), and considering ellipsoidal uncertainty on the steering vector as $(\mathbf{a} - \bar{\mathbf{a}})^H \mathbf{B} (\mathbf{a} - \bar{\mathbf{a}}) \leq 1$, the following optimization problem defines the RCB [3, 4]

$$\min_{\bar{\mathbf{a}}} \bar{\mathbf{a}}^H \mathbf{R} \bar{\mathbf{a}} \quad \text{subject to} \quad \|\mathbf{a} - \bar{\mathbf{a}}\|^2 \leq \epsilon. \quad (10)$$

It turns out the the optimal solution of Eq. (10) is when the inequality becomes equality (i.e. $\|\mathbf{a} - \bar{\mathbf{a}}\|^2 = \epsilon$). By using the Lagrange multiplier method with the multiplier denoted by $\lambda \geq 0$, the solution [3] to (10) is given as

$$\bar{\mathbf{a}} = \mathbf{a} - (\mathbf{I} + \lambda)^{-1} \mathbf{a}, \quad (11)$$

where the solution to $\|(\lambda \mathbf{R} + \mathbf{I})^{-1} \mathbf{a}\| - \epsilon = 0$ provides λ .

- **Spatial smoothing:** The Capon beamformer fails in scenarios in which the received signals are fully correlated as is the case for the ultrasound data [3, 20]. A simple formulation of spatial smoothing is used here to overcome the difficulty. Having a linear array of M transducers, the sensors are divided hypothetically into L sensors subarrays with overlapping sensors. Then, the spatial covariance matrix is the average of the covariance matrices over each of these subarrays as given by [21]

$$\hat{\mathbf{R}}(\omega_q) = \sum_{l=1}^{M-L+1} \tilde{\mathbf{y}}_l(\omega_q) \tilde{\mathbf{y}}_l^H(\omega_q), \quad (12)$$

where $\tilde{\mathbf{y}}_l(\omega_q) = [\tilde{Y}_l(\omega_q), \dots, \tilde{Y}_{l+L}(\omega_q)]^T$ is the vector of the filtered received signals through subarray l .

- **Diagonal loading:** In order to make the Capon beamformer robust to perturbation in estimating the speed of sound and also to the phase errors, a relatively small amount of white noise is added to the spatial covariance matrix. Then the spatial covariance matrix is replaced by $\mathbf{R}_{DL} = \hat{\mathbf{R}} + \sigma \mathbf{I}$ with σ being proportional to the power of received signals [22].

3. WAVE ATOM BASED COMPRESSIVE SENSING

Before image reconstruction, this paper applies CS to each of the received signals $\mathbf{y}_m = [y_m[0], \dots, y_m[N-1]]^T$ which are sampled using a $K \times N$ (with $K \ll N$) random measurement or sensing matrix Φ (as shown in Fig. 1) of the following form

$$\mathbf{x}_m = \Phi \mathbf{y}_m + \mathbf{e}. \quad (13)$$

The notation \mathbf{e} in (13) represents all measurement errors. In CS, the received signals can be reconstructed from a relatively small number of linear incoherent measurements, given the fact that the signals have sparse representation in a known basis Ψ which is incoherent with the measurement matrix Φ . In other words, the combination of $\Psi\Phi$ follows the so-called Restricted Isometry Property (RIP) [5]. Then, \mathbf{y}_m can be recovered from \mathbf{x}_m with high probability if the elements of Φ are independent realizations of a Gaussian random distribution or are following a Bernouli distribution of ± 1 . Any sparse basis that gives the best signal reconstruction for the given set of measurements can be used. For ultrasound, the researchers have used several different basis functions like Fourier, wavelet and wave atom. The quality of recovery depends mostly on (i) choosing the best basis in which the signals have the most sparse representation; and (ii) the ratio of the number of compressed measurements acquired to the number of information bearing (non-zero) components of the signal in that basis. Recently, Demanent and Ying [10] showed that wrapped oscillatory patterns like ultrasound waves have sparse representation in the wave atom basis. Following [11,23] and as shown in the third block of Fig. 1, the wave atom dictionary is applied to represent the ultrasound RF signals in the sparse domain. But in recovery, instead of using the traditional l_1 -norm or Basis Pursuit, the optimization problem used here is based on regularized- l_1 [24] which can be written as

$$\text{minimize } \tau \|\Psi^T \mathbf{y}_m\|_1 + \frac{1}{2} \|\Phi \mathbf{y}_m - \mathbf{x}_m\|_2^2 \quad (14)$$

with $\tau > 0$ being the regularization parameter. The l_1 -regularization term in (14) promotes Ψ -domain sparsity in the solution and the l_2 -norm term keeps the solution close to the measurements. The NESTA algorithm [15] is used to solve the optimization in (14) suitable for ultrasound signals with high dynamic range. The regularization parameter τ is selected empirically based on a trade off between the quality of reconstruction and the speed of convergence.

4. EXPERIMENTATION

To investigate the performance of the proposed approach, three different test environments are used based on simulations, phantom data, and real *in vivo* cardiac data. For the simulation phase, the Field II simulator [25] is used with four strong point reflectors in a free-space with a sound velocity of 1540m/s. The transducers centre frequency is 3.5MHz and a linear array of 128 rectangular transducers are used in the simulation. The width of the transducers are 440 micron with height of 5mm and kerf of 0.05mm. The excitation is a sinusoidal signal with a sampling frequency of 50MHz. A full

data matrix is captured. The received data from each transducer is sampled using the Bernouli projection matrix producing 1/8th of the samples. Then each of the signals being projected by the sensing matrix is recovered using wave atom dictionary which is optimized based on (14) with τ selected to be 0.02. The reconstructed signals are used by the Capon algorithm to form the final image. Since the exact locations of the arrays are known, the standard Capon algorithm is used with a diagonal loading. Figure 2(a) shows the result of beamforming with the original RF data at the transducer array and using the Capon algorithm whereas Figure 2(b) is the reconstructed image taking 1/8 of the samples used in the first figure based on the regularized- l_1 CS recovery method. Both figures show the locations of the reflectors correctly. Using an experimental ultrasound data, the same methods are applied to the digital raw data acquired from a wire phantom. The received signals were captured with a 128-channel receiver (SonixDAQ, Ultrasonix, Richmond, B.C., Canada) at the centre frequency of 6MHz as shown in Fig. 3(a). Fig. 3(b) shows the image of the wires using the RCB method with $\epsilon = 4$ after beamforming without CS and with 20MHz sampling frequency. For quantitative comparisons, the structural similarity (SSIM) index [26] in the resulted image and the normalized root mean square errors (NRMSE) in the reconstructed signals are often used to measure similarity between two images or two signals [8]. We compute the SSIM for subplots (b) and (c) in Fig. 3 which is 0.9 for the wire phantom and the NRMSE to be 0.0504 for the reconstructed signals. Since a higher value of SSIM implies a greater level of similarity between the images, using CS results in some degradation in the quality of the image reconstruction. Finally, the same method is applied to the real cardiac data obtained from an ultrasound machine. While the RCB based generated image is shown in Fig. 4(a), the recovered image from 1/6th of the samples is shown in Fig. 4(b). Considering the speckle noise structure that exists in the original image, both the NRMSE and SSIM became 0.164 and 0.703 for the reconstructed image (subplot (b)).

5. SUMMARY

In this work, a wave atom based CS method is applied to reconstruct a 2D image from samples taken at a reduced rate compared with conventional sampling rates used in ultrasound machines. A robust adaptive beamforming technique is used on the recovered signals for beamforming coupled with spatial smoothing to deal with coherent sources, and diagonal loading to deal with medium uncertainties. Experimenting with a wire phantom and *in vivo* cardiac data show that it is possible to get the same quality image (with NRMSE of 0.164 and with SSIM of about 0.7) using only 10% – 20% of the samples used in the conventional beamforming.

Acknowledgement

The author would like to thank Prof. P. Abolmassoumi from University of British Columbia, Canada for providing data to test our algorithms.



Fig. 2. Field II simulated program with four point scatterers and 128 elements uniform linear array of transducers. (a) image reconstructed with the Capon beamformer and (b) image reconstructed with the CS recovery based on the regularized- l_1 method followed by applying the Capon beamformer to the recovered signals. Both figures used the same 30-dB display dynamic range.

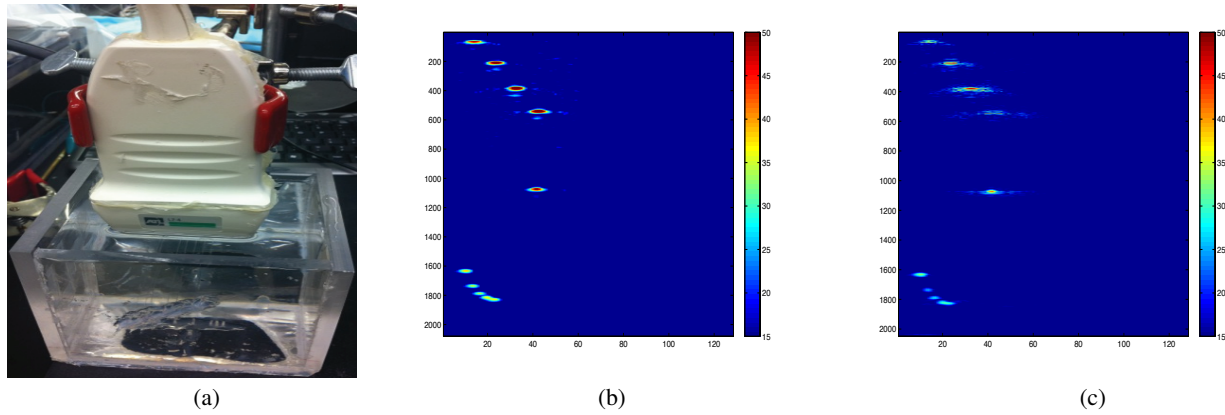


Fig. 3. Experimental ultrasound setup for the wire phantom with $M = 128$ (a), (b) image reconstructed with the robust Capon beamformer and (c) image reconstructed with the CS recovery using the regularized- l_1 and the RCB.

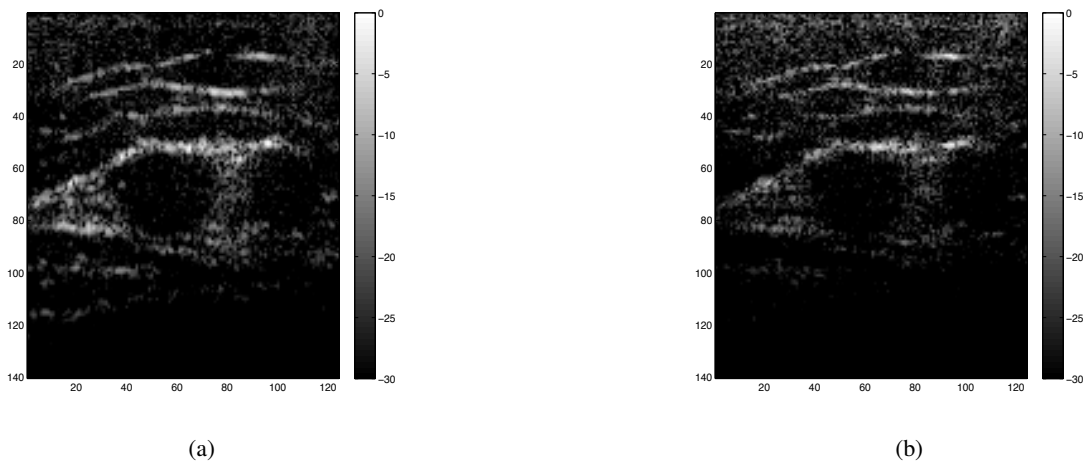


Fig. 4. Experimental cardiac images: (a) Heart image reconstructed with the robust Capon beamformer and (b) image reconstructed with the signals generated from a random Bernoulli sensing matrix with 1/6th of the machine generated samples and recovered using the CS recovery. The reconstructed signals are beamformed using the RCB to form the image with $\epsilon = 5$ and 30-dB display dynamic range.

6. REFERENCES

- [1] S. Holm, J.-F. Synnev, and A. Austeng, "Capon beamforming for active ultrasound imaging systems," in *Digital Signal Processing Workshop and 5th IEEE Signal Processing Education Workshop*, Jan 2009, pp. 60–65.
- [2] S. J. Norton and I. J. Won, "Time exposure acoustics," *IEEE Transactions on Geoscience and Remote Sensing*, vol. 38, no. 3, pp. 1337–1343, 2000.
- [3] P. Stoica, Z. Wang, and J. Li, "Robust Capon beamforming," *IEEE Signal Processing Letters*, vol. 10, no. 6, pp. 172 – 175, 2003.
- [4] Z. Wang, J. Li, and R. Wu, "Time-delay-and time-reversal-based robust Capon beamformers for ultrasound imaging," *IEEE Transactions on Medical Imaging*, vol. 24, no. 10, pp. 1308–1322, 2005.
- [5] E. Candes, J. Romberg, and T. Tao, "Robust uncertainty principles: exact signal reconstruction from highly incomplete frequency information," *IEEE Transactions on Information Theory*, vol. 52, no. 2, pp. 489–509, Feb 2006.
- [6] D. L. Donoho, "Compressed sensing," *IEEE Trans. Inform. Theory*, vol. 52, pp. 1289–1306, 2006.
- [7] N. Wagner, Y. Eldar, A. Feuer, and Z. Friedman, "Compressed beamforming with applications to ultrasound imaging," in *2012 IEEE International Conference on Acoustics, Speech and Signal Processing (ICASSP)*, March 2012, pp. 3641–3644.
- [8] N. Wagner, Y. Eldar, and Z. Friedman, "Compressed beamforming in ultrasound imaging," *IEEE Transactions on Signal Processing*, vol. 60, no. 9, pp. 4643–4657, Sept 2012.
- [9] T. Chernyakova, Y. Eldar, and R. Amit, "Fourier domain beamforming for medical ultrasound," in *2013 IEEE International Conference on Acoustics, Speech and Signal Processing (ICASSP)*, May 2013, pp. 924–928.
- [10] L. Demanet and L. Ying, "Wave atoms and sparsity of oscillatory patterns," *Applied and Computational Harmonic Analysis*, vol. 23, no. 3, pp. 368 – 387, 2007.
- [11] D. Friboulet, H. Liebgott, and R. Prost, "Compressive sensing for raw RF signals reconstruction in ultrasound," in *Ultrasonics Symposium (IUS), 2010 IEEE*, Oct 2010, pp. 367–370.
- [12] E. Candes and T. Tao, "Decoding by linear programming," *IEEE Transactions on Information Theory*, vol. 51, no. 12, pp. 4203–4215, Dec 2005.
- [13] J.-P. Antoine and R. Murenzi, "Two-dimensional directional wavelets and the scale-angle representation," *Signal Processing*, vol. 52, no. 3, pp. 259 – 281, 1996.
- [14] S. Mallat, *A Wavelet Tour of Signal Processing, Third Edition: The Sparse Way*, 3rd ed. Academic Press, Dec. 2008.
- [15] S. Becker, J. Bobin, and E. J. Candès, "NESTA: A fast and accurate first-order method for sparse recovery," *SIAM J. Img. Sci.*, vol. 4, no. 1, pp. 1–39, Jan. 2011.
- [16] M. Gyöngy and C.-C. Coussios, "Passive cavitation mapping for localization and tracking of bubble dynamics," *The Journal of the Acoustical Society of America*, vol. 128, no. 4, pp. EL175–EL180, 2010.
- [17] J. Li and P. G. Stoica, Eds., *Robust adaptive beamforming*, ser. Wiley series in telecommunications and signal processing. Hoboken, NJ: John Wiley & sons, 2006.
- [18] J. Capon, "High-resolution frequency-wavenumber spectrum analysis," *Proceedings of the IEEE*, vol. 57, no. 8, pp. 1408 – 1418, August 1969.
- [19] N. J. Roseveare and M. R. Azimi-Sadjadi, "Capon beamspace beamforming for distributed acoustic arrays," *Unattended Ground, Sea, and Air Sensor Technologies and Applications IX*, vol. 6562, p. 65620K, 2007.
- [20] J.-F. Synnev, A. Austeng, and S. Holm, "Adaptive beamforming applied to medical ultrasound imaging," *IEEE Transactions on Ultrasonics, Ferroelectrics and Frequency Control*, vol. 54, no. 8, pp. 1606–1613, August 2007.
- [21] L. Zhang and W. Liu, "Robust beamforming for coherent signals based on the spatial-smoothing technique," *Signal Process.*, vol. 92, no. 11, pp. 2747–2758, Nov. 2012.
- [22] J. Li, P. Stoica, and Z. Wang, "On robust Capon beamforming and diagonal loading," *IEEE Transactions on Signal Processing*, vol. 51, no. 7, pp. 1702–1715, July 2003.
- [23] H. Liebgott, A. Basarab, D. Kouame, O. Bernard, and D. Friboulet, "Compressive sensing in medical ultrasound," in *Ultrasonics Symposium (IUS), 2012 IEEE International*, Oct 2012, pp. 1–6.
- [24] M. Asif, F. Fernandes, and J. Romberg, "Low-complexity video compression and compressive sensing," in *2013 Asilomar Conference on Signals, Systems and Computers*, Nov 2013, pp. 579–583.
- [25] J. Jensen, "Simulation of advanced ultrasound systems using Field II," in *2004 IEEE International Symp. on Biomedical Imaging: Nano to Macro*, April 2004, pp. 636–639 Vol. 1.
- [26] Z. Wang, A. Bovik, H. Sheikh, and E. Simoncelli, "Image quality assessment: from error visibility to structural similarity," *IEEE Transactions on Image Processing*, vol. 13, no. 4, pp. 600–612, April 2004.